Mur ligases binding site analysis and in silico modulation of the fragments targeting MurD ligase allosteric binding site

SN: 18022860

ABSTRACT: A group of enzymes called Mur ligases are involved in the intracellular pathway of bacterial peptidoglycan biosynthesis. They are one of the most appealing targets for antibacterial drug discovery. Although many studies have focused on the various binding sites including ATP and substrate binding sites, there are no known lead compounds that have been developed into medicine. With the development of fragment screening by X-ray crystallography, four fragment hits were identified to bound with a new allosteric binding pocket. Fragment 373 was selected for further investigations. After two rounds of experiments, including moieties selection and in silico modulation, compounds 18,19,20,21 were proved to have lower binding energy and better ligand-protein interactions performance.

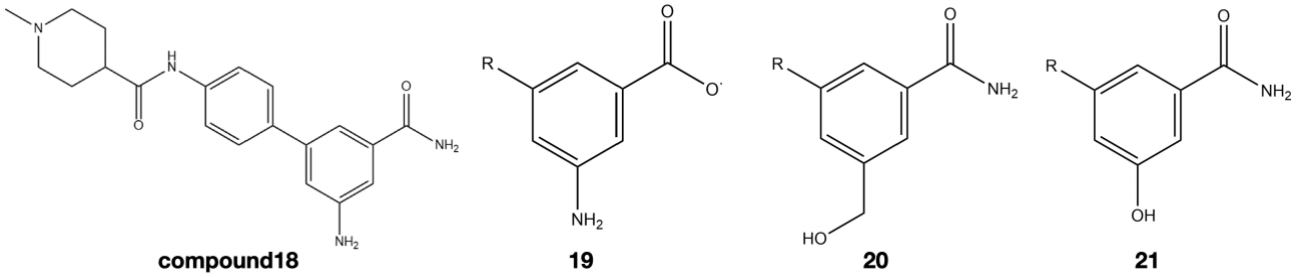

Background information:

Antimicrobials are used to fight against pathogenic bacteria. However, with the increase in the use of antibacterial drugs, the level and complexity of the resistance mechanisms exhibited by bacterial pathogens have also elevated. [1] Antimicrobial-resistant infections are estimated to kill 700,000 people each year and are expected to kill 10,000,000 people annually by 2050. These would cost $100 trillion if there is no effective action. [2] This urgently demands new research and data on potential targets and the development of novel effective medicine in this field. [3]

Most bacterial cell walls contain peptidoglycan (PG), which provides the flexibility, strength, and rigidity necessary for bacterial cell growth and division while also being able to withstand high internal osmotic pressure. [4] This rigid scaffold consists of peptides and sugar molecules. The structure is essential and unique for maintaining the structural integrity of the cell in both gram-negative and gram-positive bacteria. [4,5] In the past decade, many studies have focused on discovering new antibacterial drugs by exploiting enzymes involved in the biosynthesis of early intracellular cytoplasmic peptidoglycan precursors. [5, 13, 14, 20, 21, 23, 24]

The enzymes called Mur ligases are involved in the initial PG synthetic steps. First, the transferase MurA cleaves the enol pyruvate moiety from phosphoenolpyruvate (PEP) to form UDP-n-

This project is a Type B Systematic review with chosen Hypothesis with a word count of 4240 words formatted in the printed style of *Journal of Medicinal Chemistry*

acetylglucosamine (UDP-GlcNAc). [8, 9] Then, the reductase MurB, with the assistance from the cofactor NADPH, reduces the enol pyruvate moiety to a lactyl group and finally results in the formation of UDP-N-acetylmuramic acid (UDP-MurNAc). [8, 10] Follow-up is the construction of the pentapeptide side chain, which involves the addition of five amino acids by a different enzyme. The first step is the condensation of two D-Ala molecules through enzyme Ddl. Then, the L-Ala, D-isoGlutamate, and Meso-Diaminopimelic acid are added sequentially by MurC MurD and MurE. After that, the MurF enzyme adds the D-Ala-D-Ala dipeptide to the m-DAP, finally forming a pentapeptide side chain. (refer to Figure1) [6, 7, 8, 11]

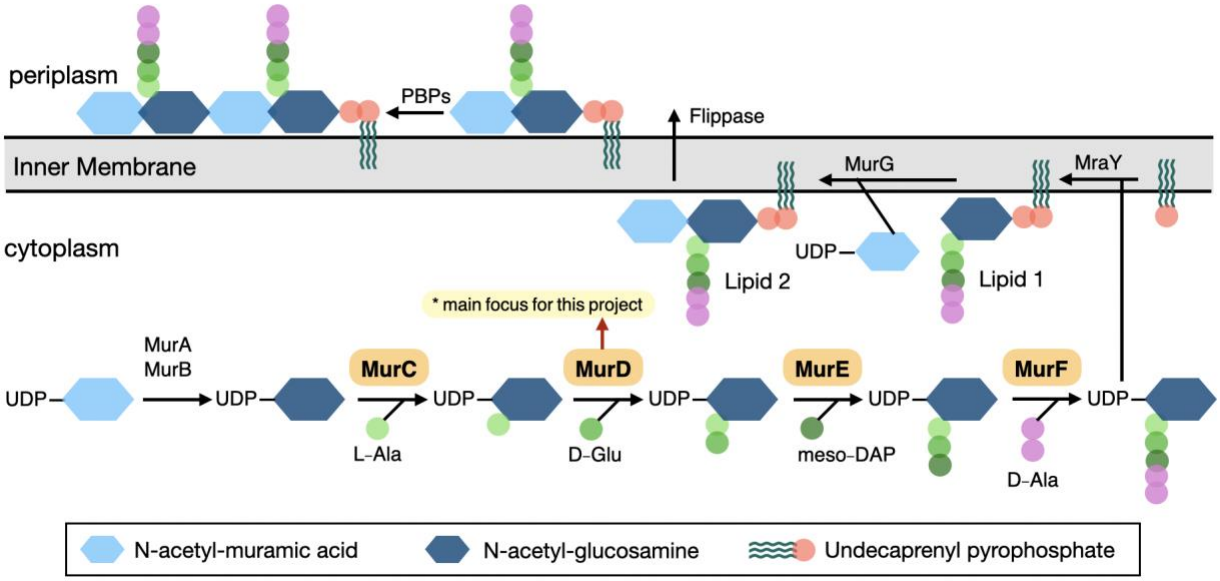

Figure 1: Scheme of the peptidoglycan synthesis process (The target Mur ligases are highlighted in orange boxed) [8]

Among these Mur ligases, the crystal structures of Mur C/D/E/F from various bacterial species share a generally similar three-domain topology especially for the central and C-terminal domains which bind to ATP or GTP-ases and condensed amino acids or dipeptide residue. [11,12,13] In contrast, the N-terminal domain is involved in combination with the UDP precursor, and this domain presents some differences between MurC/MurD and MurE /MurF. [12,13,14] MurC and MurD share a common Rossmann-type α/β fold at the N-terminal domain. On the other hand, MurE and MurF, have α/β fold with different topology and a mixed β-sheet compared with the all-parallel β-sheet in MurC and MurD. In addition, the way the two groups of enzymes bind to the UDP substrate in significantly different ways. This difference in folding and binding may be related to a series of reactions on extended substrates catalyzed by Mur ligase. [13,14] All four enzymes are essential for bacterial survival; thus, the inhibitors of the Mur ligases would interfere with the cell integrity and present an antimicrobial effect. Overall, MurC/D/E/F share a very similar structure, making them an appealing drug target. Since there is a higher potential for the lead compounds to perform a multiple inhibition effect. (refer to Figure 2)

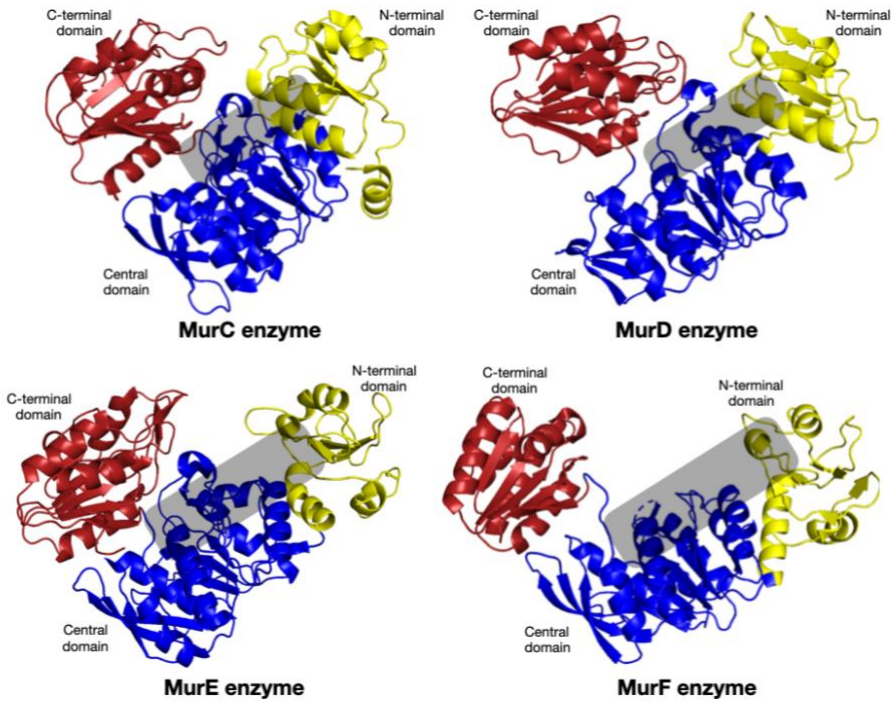

Figure 2: Crystal structure of the *E. coli* MurC (PDB code: 2F00)/MurD (PDB code: 2UAG)/MurE (PDB code: 2E8C)/MurF (PDB code: 1GGA) enzyme, N-terminal domain is denoted in yellow, central domain in blue and C-terminal domain in red. The grey shadow box illustrates the substrate-binding site.

ATP binding sites of Mur ligases

The reaction mechanism scheme for MurC-F ligases also shares some generality, especially for MurC and MurF which have already been firmly confirmed. [12,13,14] To start with, ATP initially activates the carboxyl group of the UDP precursor to produce acyl phosphate intermediate and ADP. [17,18] Then the nucleophilic attack of the amino group from the incoming condensing amino acid or dipeptide (R′ -NH2) leads to the formation of tetrahedral intermediate with high energy. [15,16] Finally, the phosphate group is dissociated from the tetrahedral intermediate, giving the final product peptide (R-CO-NH-R′), which is a new UDP precursor elongated by the condensation of amino acid, amide, and phosphate. [12, 15] (refer to Figure3)

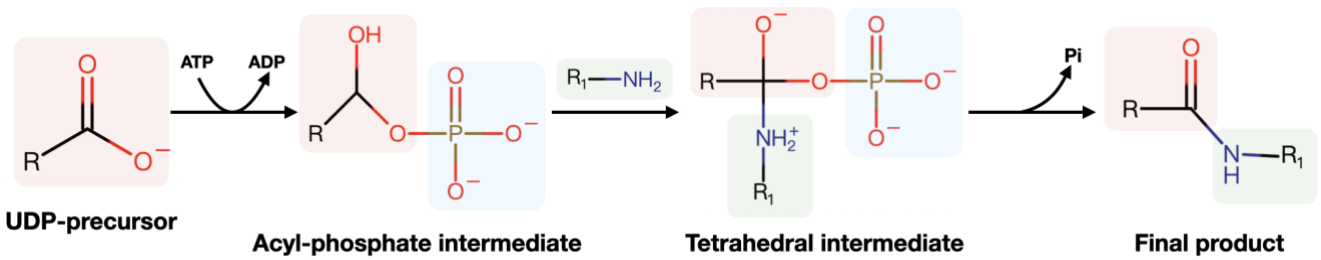

Figure3: The general reaction mechanism scheme for MurC-F ligases. [16, 20]

In general, MurC/E/F ligases are all ATP-dependent. Furthermore, whether it is a horizontal comparison of Mur ligase in the same strain or a vertical comparison of the same Mur ligase in different strains, ATP binding sites have shown very high alignment (refer to Figure 4). This characteristic makes this binding site an appealing target for novel inhibitors. This is because if the lead compound targets the ATP binding pocket of one of the enzymes and is able to inhibit the enzymatic action of Mur ligase. The similarity among the ATP binding sites suggests that the compound also has the probability to inhibit the other three remaining enzymes. A multiple inhibition effect would lead to delayed antimicrobial resistance.

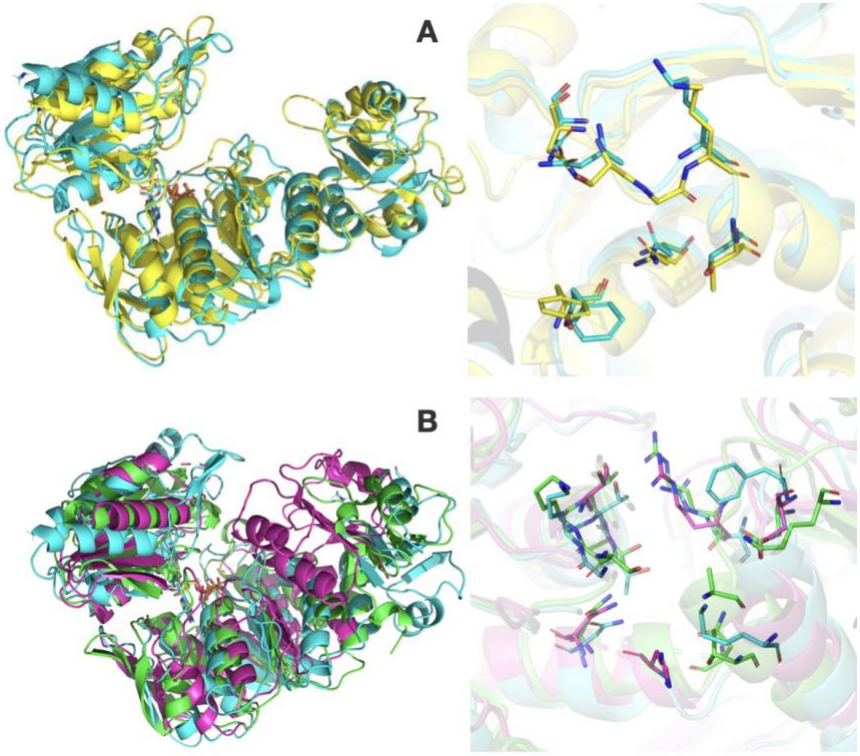

Figure4: (A) Left side: Structural superposition of MurD ligases from different bacteria strains. Right side: ATP binding site alignment of MurD ligases from different bacteria strains. *Mycobacterium tuberculosis* MurD is shown in yellow (PDB code: 2XJA); *Thermotoga maritima* MurD is shown in light blue (PDB code: 4BUB) (B) Left side: Structural superposition of different Mur ligases of the same strains-*Thermotoga maritima*. Right side: ATP binding site alignment of Mur ligases from *Thermotoga maritima*. MurC is shown in purplish red (PDB code: 1J6U); MurD is shown in light blue; (PDB code: 4BUB) MurF is shown in green (PDB code: 3ZL8) (prepared by PyMol [19])

However, targeting the ATP binding site of Mur ligases is still challenging. The inhibitors that bind to the ATP-binding site must be selective for target bacterial enzymes, not human ATP-dependent enzymes, especially kinases. Otherwise, even if the compounds can achieve a suitable therapeutic dose, the serious adverse drug effects during the clinical trial might terminate the process of formulating the compounds into drugs. Other than that, the original ATP concentration in the bacterial cell is 0.6–18 mM. This remarkably large amount of ATP would compete with the drug compounds and make the binding more difficult. Also, the amount is similar to that in human cells which is 1–10 mM. [20] In addition, the kinetic mechanism of MurD presents some randomness, especially considering that the molecular isotope exchange reactions are not strictly ADP-dependent. [16]

Despite extensive research in this field, no Mur ligase ATP binding site inhibitor known until now can be applied therapeutically, [20] indicating that other binding sites should be considered.

Substrate binding sites of Mur ligases

Another prevalently researched binding pocket is the substrate-binding site. However, the previous study [25] revealed that MurD has an inherent feature where the C terminal domain will flip to the top and slightly change the residues around the UMA substrate. (refer to Figure5) Whereas most of the substrate mimic compounds were large molecules. Compared to fragments, larger molecules are more complex. As a result, small adjustments to the atoms can lead to large changes in the binding pose, with the result that the compound loses key interactions. The weakened binding affinity would destroy an otherwise perfectly binding compound. Complex conformation change may be a partial explanation for most compounds failure when tested in vivo and in vitro. Poor cell penetrance and high intracellular concentrations of competitive substrates or cofactors might also be the underlying causes. [25]

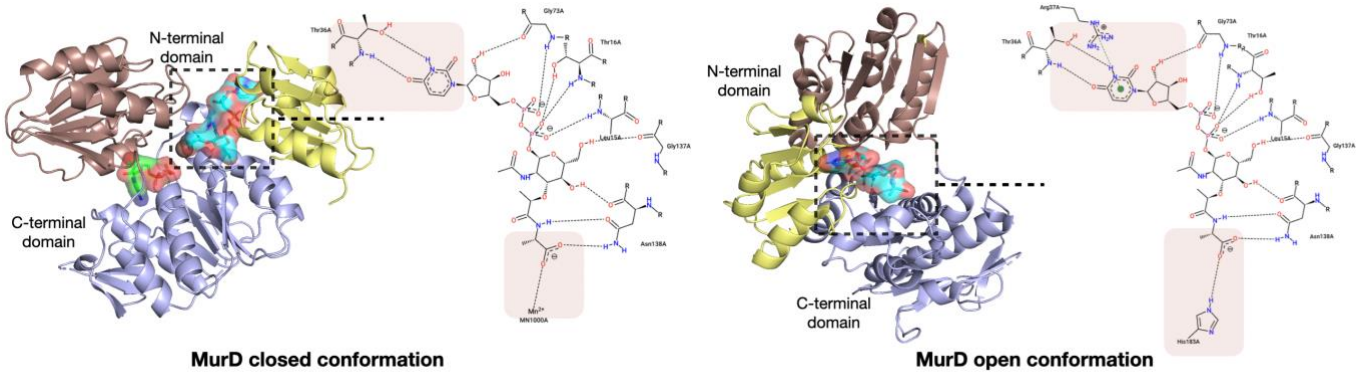

Figure4: Left side: closed conformation for E coli. MurD (PDB code: 2UAG) Right side: the open conformation for E coli. MurD (PDB code: 1EEH). The UMA binding site is shown in light blue, the differences in surrounding residues are shown in pink shadow boxes. (3D diagram is prepared by PyMol [19], the 2D diagram is prepared by Protein Plus [33,34])

Most inhibitor drug design projects of Mur ligases are structure-based and mainly focused on compounds that target the ATP substrate binding site and binding site, but only a limited number of ligands could be crystallized within the Mur ligase active sites. [13, 14, 20, 21, 23, 24] Therefore, targeting secondary or allosteric binding sites may be a new approach. The emerging of novel drug discovery approaches and the development of screening platforms and technology can help scientists to identify more possible compounds with the potential to become effective drugs in the future.

Fragment-based drug discovery

Fragment-based drug discovery is a method used to find lead compounds, normally small molecules, in the drug design process and is a viable alternative to conventional high-throughput screening. It starts with identifying small chemical fragments that may only weakly bind to biological targets and then grow or bind them to produce lead candidates with high affinity (refer to Figure6).

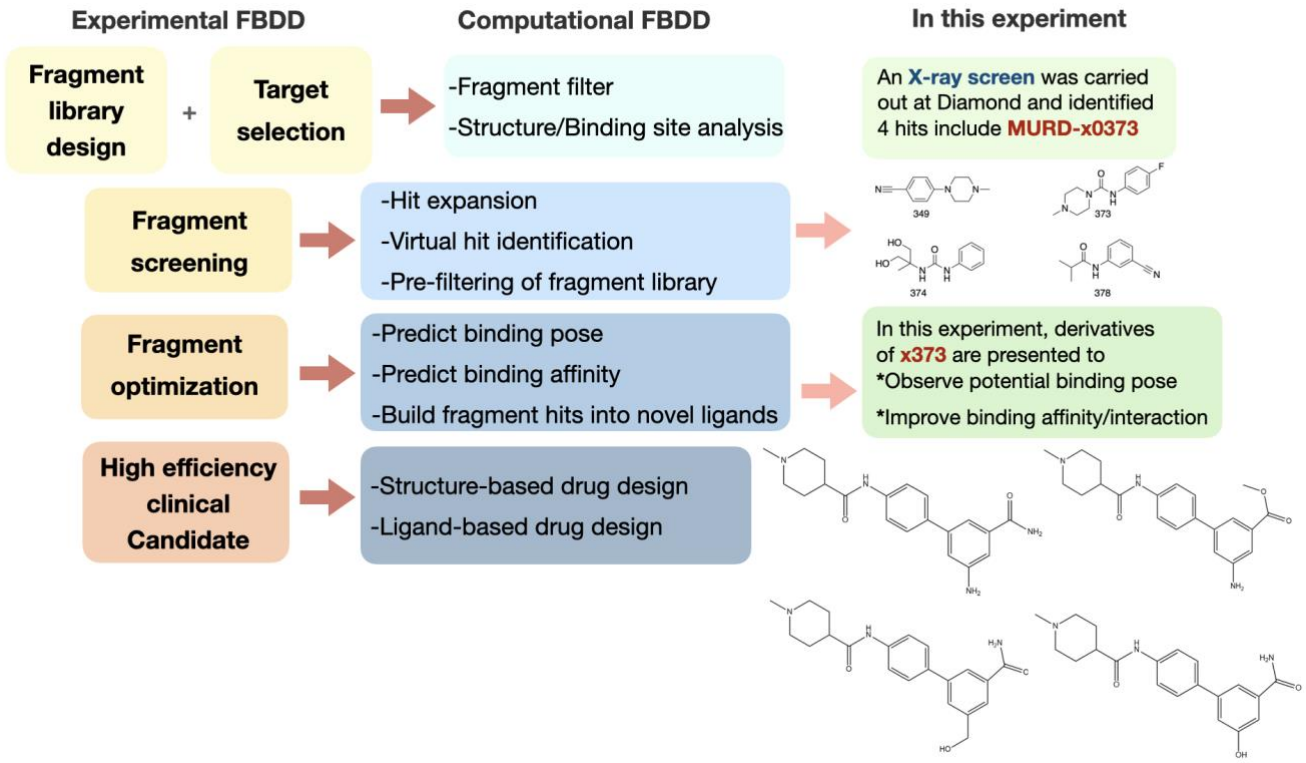

Figure6: Complementary relationship between experimental (shown in yellow) and computational (shown in blue) fragment-based drug design. The green section summarizes the scheme for the sequential experiment. [26]

Fragments generally refer to those organic molecules with small size and low molecular weight and typically contain less than 20 non-hydrogen atoms. Therefore, the fragment-based drug discovery considerably reduces the number of possible compounds, compared with the huge number of drug-like compounds with up to 30 heavy atoms. [26,27] In addition, larger ligands have a higher potential to form more interactions with surrounding residues, which could increase the binding affinity indeed. [28] On the contrary, more interaction also indicates that even a single misplaced atom can destroy a probable fitting compound. Other than that, fragments sample the binding properties of a protein more comprehensively, which leads to a generally more efficient hit rate than HT screens. [29]

In spite of the above advantages, the design of fragment-based drugs has certain limitations. Fragments, due to their small molecular weight, inevitably lead to a reduction in the binding affinity of the compound to surrounding residues. This, in turn, means that the binding between fragments and proteins is usually more difficult to detect. In addition, high concentrations of compounds will interfere with the results of the test, making it more challenging to observe the docking results. Thus, new technology, such as fragment screening by X-ray crystallography, has been developed and proved to circumvent these problems to a certain extent. [30,31,32] When using this technique, only the compound's solubility is limited. [31] Furthermore, it is unlikely that false positives will come out of X-ray crystallographic screening because of the immediate visualization of protein-fragment interactions. [32] However, due to its limited production, it has rarely been used as the main screening method until now.

Allosteric binding sites

By applying the strategy discussed above, the contributors of the project from Warwick screened 56 fragments against MurD ligase from Streptococcus agalactiae serogroup. The first round of experiments was conducted to test the antibacterial activity of those fragments. Then 4 original fragment hits were identified by carrying out the X-ray screen at Diamond (refer to Figure7). [37]

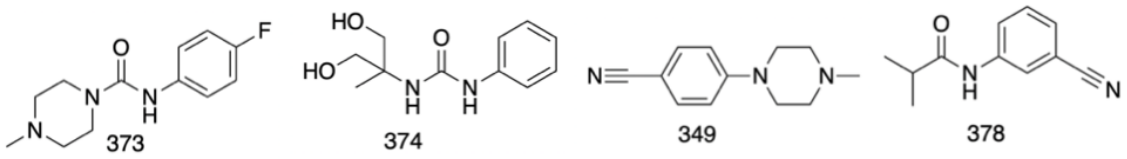

Figure7: Four identified fragment hits from.

These four fragments are bound in the allosteric binding site which is located between the C-terminal and central domain. This binding site is remote from the substrate UMA binding pocket and adjacent to the site where ADP is bound in the E. coli crystal structures. The experiment in this study focuses on the original fragment 373. This fragment displays several important interactions with the surrounding residues (refer to Figure8). [36]

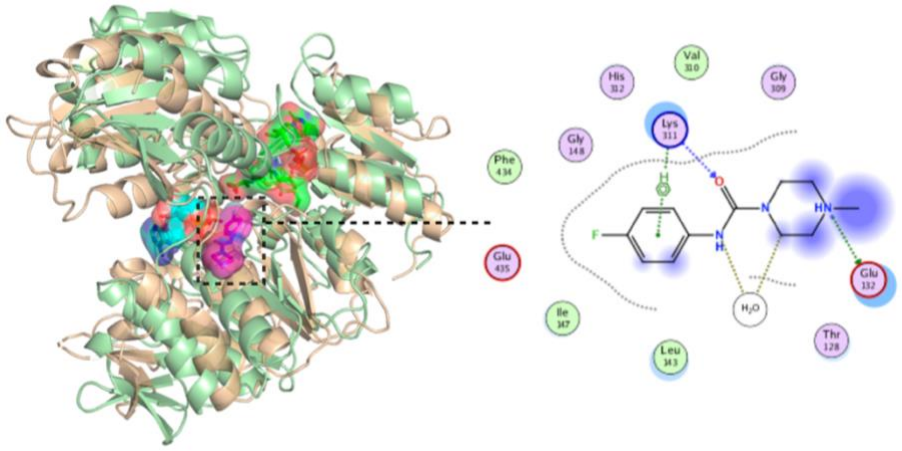

Figure8: Left side: the alignment for E coli MurD ligase shown in wheat (PDB code: 3uag) and Streptococcus agalactiae serogroup MURD with fragment x0373 complex shown in pale green (PDB code: 3LK7). The allosteric binding site is shown by the magenta surface, the ATP binding site is shown by the blue surface, the substrate UMA binding site is shown by the green surface. Right side: the ligand-protein interaction diagram prepared by the 'MOLECULAR OPERATING ENVIRONMENT'. [35]

Within the binding pocket, the phenyl ring is surrounded by the residues Glu435, Phe434, Gly148, Ile147, His312 and Lys311. This moiety forms pi-pi interaction with the Lys311, which the backbone NH of this residue also hydrogen-bonded with urea carbonyl group located between the phenyl and piperazine. For the part where the fragment is exposed to solvent majorly, nitrogen atom from the protonated piperazine nitrogen forms interaction with Glu132.

Before the present project, a round of elaboration on the fragment hits had already been done by the previous contributor from the project. The results reveal that there are several advantages for changing the piperazine to piperidine. (refer to Figure9)

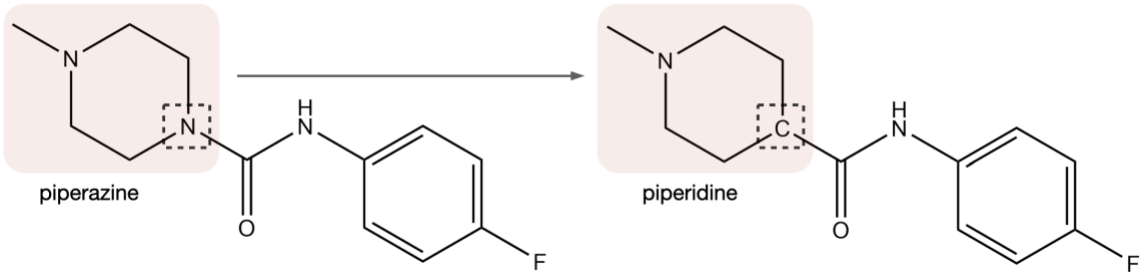

Figure9: Change the piperazine to piperidine by replacing the nitrogen atom with the carbon atom.

First, the nitrogen modulated does not form any essential interaction with the surrounding residues. In addition, the top nitrogen is protonated, and hydrogen boned with Glu312. This atom in piperidine is estimated to have higher basicity than in piperazine, which suggests a stronger interaction. Finally, from the experimental perspective, the piperidine would be easier to synthesize. The inhibitory activity of the elaborated fragment library in the first round was tested against MurD, and the results confirmed this hypothesis because some piperidine-containing fragments are effective. [36]

The aims of this project were to observe the structure of the original fragment 373 and expand the fragments into lead compounds with higher potencies and molecular weights. The fragment growing can be done by the attachment of various moieties. To start with, from visual observation, the size of the new determined allosteric binding pocket is not large. Therefore, the modulated compounds must ensure that they can fit into the binding pocket. Then the different docking configurations should be compared visually. By observing the binding poses, we could analyze whether the suggested compounds align with the original fragment. Then the RMSD value is calculated to confirm the level of alignment. These compounds should be able to keep as much important interaction as possible and try to increase the binding affinity between the ligand and the residues within the binding site. The compounds with the lowest binding energy and highest interactions were selected for further evaluations, including the steady-state kinetic evaluation and the antibacterial activity determination.

Materials and methods

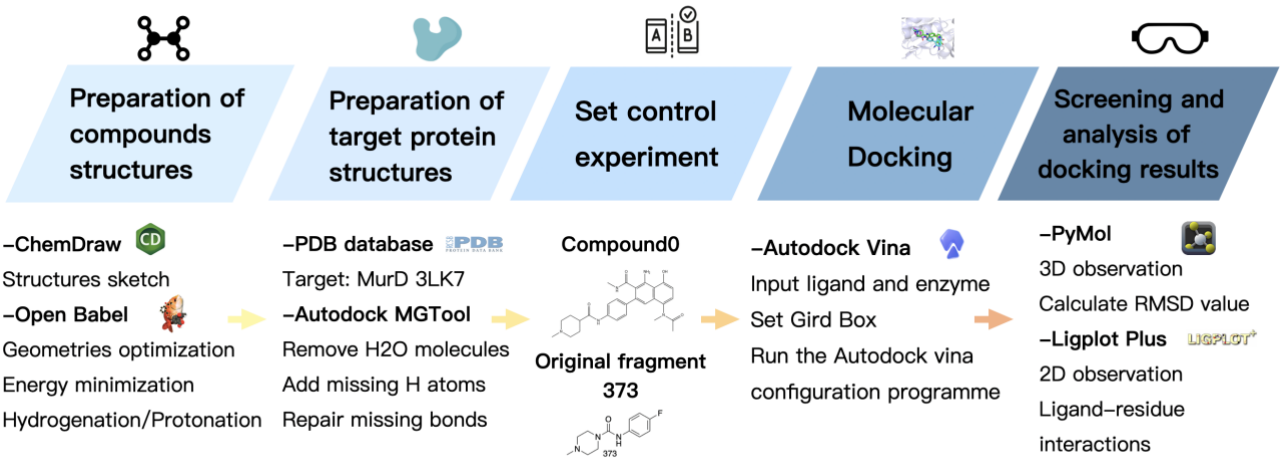

Figure10: Schematic presentation of the experimental process, including the major steps and all the computational resources and software (with symbols behind).

Preparation of small molecular structures

The first section of the experiment involves the docking of compounds 1-11, suggested by another contributor from the project, which is derived from the original fragment MURD-x0373. Then, according to the results from the first section, the moieties that have the greatest potential of forming interactions with surrounding key residues were sorted out and then create new compounds by modulating the previous ligands. [38]

The structures of compounds 1-18 were sketched using ChemDraw, and then all the structures were imported into Open Babel for structure and geometries optimization, hydrogenation, and energy minimization. In this case, compounds' protonation is also required for maintaining the potential interaction between surrounding residue Glu132 and the piperidine nitrogen atom. Only then are the compounds ready for molecular docking. [39]

Preparation of target protein structure

MurD ligase (PDB code: 3LK7) from the PDB database is selected as the target form docking, and the protein structure was processed on the Autodock MGTool platform. The actions include the removal of water molecules that do not surround the binding site, the addition of the missing hydrogen atoms, and the repair of a few missing bonds. Finally, protein-energy minimization and geometric structure optimization were carried out. [40,41]

Set control experiment

The original fragment 373 and compound 0 (refer to Figure 9) were set as a control experiment to test against the software parameters and performance with all variable factors. These include the position of the grid box and the operation process of docking software, which had to be kept constant. The results showed that fragment 373 docked to the target binding site with RMSD value=0.018 when it is aligned

with the 373 from the crystal structure MurD-x373. Oppositely, the negative control compound 0 failed to dock into the binding pocket. [19,40,41]

Molecular Docking

Molecular docking was done using the Vina plug-in module in Autodock software, and the protein and molecules were inputted into the Autodock MDTool. As illustrated in Figure 9, the grid box was set (refer to Figure11) to a precise shape and position to ensure the configurations presented in the results resemble the original fragment MURD-x0373. Thus, this process, along with the protonation in 1.1, can help save as many crucial interactions as possible. Each ligand-enzyme docking was run by Autodock vina twice to guarantee that the maximum binding affinity difference between two sets of outcomes is within ±0.1 KJ/mol. [40,41]

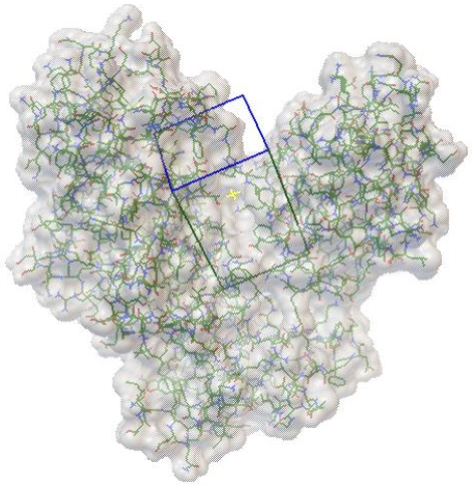

Figure11: The grid box is marked by cuboids with thick blue lines. The aim of this setting is to restrict the position of the molecule binding and ensure that the final docked pose can be highly aligned with the original fragment.

Screening and analysis of docking results

The best-ranked docking results, including those compounds with the lowest binding energy, were selected, and imported into PyMol for further visual inspection. Then the RMSD value is calculated using the ‘align’ command. As shown in Figure12, two configurations were identified as references. The poses with RMSD values less than 1.5 Å have more alignment consistency with fragment 0373 and were selected for further residues interaction analysis. After the above two rounds of screening, the remaining configurations were imported into Ligplot for ligand-enzyme interaction analysis. [19,42,43]

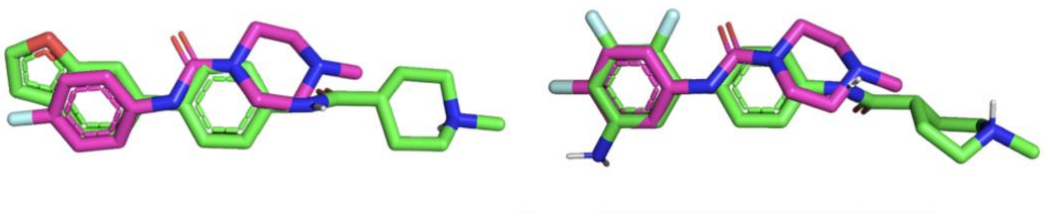

Figure:12 The second configuration of compound 5 and the third configuration of compound 7 are shown in green, while the original fragment 373 is shown in purple. Left side: Alignment of original 373 hit fragment with

the 2nd configuration obtained by docking of compoun5 with 3LK7: The reason for setting this pose as reference is due to the highly resemble of the position of the aromatic ring, which is inserted into the binding site with the original 373 by visual observation. Right side: Alignment of original 373 hit fragment with the 3rd configuration obtained by docking of compoun7 with 3LK7: The reason for setting this pose as reference is due to the highly resemble of the backbone and direction with the original 373 by visual observation.

Results and discussion:

Experiment Part1

The first part of the experiment focuses on observing the binding poses generated by compounds 0-11 and selecting the moieties which have the highest potential to form stronger interactions with surrounding residues and increase the binding affinity between the compounds and the binding pocket. The results obtained by Autodock vina [39,40] are shown in Table 1 and the 2D structures for the compounds are shown in the diagram. (refer to Figure13) Then the complexes of proteins and compounds were visually analyzed by Pymol2.1 and Liglplot Plus.

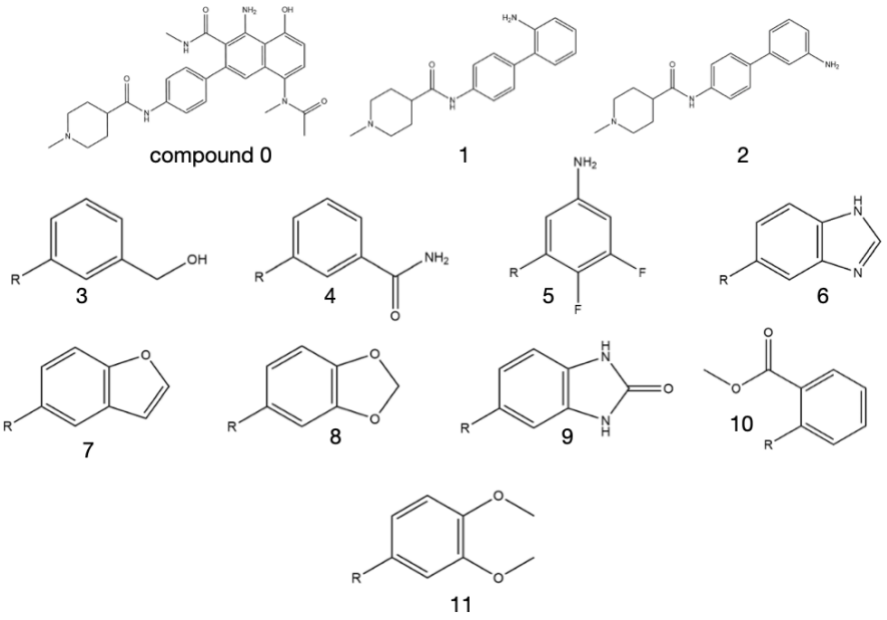

Figure13: The 2D structures for compounds 0-11

Table1. Targets protein docking results for compounds 0-11

Compound Number	Configuration Number	Binding energy	RMSD value C5-conf2 / C7-conf3	Hydrogen bonded Residues
0	The compound 0 is set as a control experiment, it does not have any docking results.			
1	1-1	-7.2	1.768/0.147	NA
	1-2	-7.1	1.533/0.521	Glu132
	1-3	-6,6	1.353/0.767	NA
	1-4	-6.6	1.906/1.515	Thr128

2	2-1	-6.8	1.602/0.175	Gly148
	2-2	-6.7	0.109/0.359	Glu132/Lys311
	2-3	-6.6	1.261/1.043	NA
	2-4	-6.4	1.260/0.837	Lys311
3	3-1	-7.0	0.133/0.285	Glu132
	3-2	-6.8	0.191/0.860	Lys311
	3-3	-6.5	0.169/0.801	Glu132/Glu435/ Gly148
4	4-1	-7.3	1.317/1.122	Thr128
	4-2	-7.0	0.243/0.523	Glu132/ Thr128
	4-3	-6.9	0.243/0.523	Glu132/ Thr128
5	5-1	-6.8	0.786/0.933	Glu132/ Thr128
	5-2	-6.7	NA/0.457	Glu132/ Thr128
	5-3	-6.6	0.023/0.867	Glu132/ Thr128/ Gly148
6	6-1	-7.3	1.296/1.494	Glu132
	6-2	-7.1	0.115/0.398	Glu132
	6-3	-6,8	0.396/0.161	NA
7	7-1	-7.5	0.974/0.114	Glu132
	7-2	-7.2	0.953/0.499	Glu132
	7-3	-7.0	0.457/NA	Glu132
8	8-1	-7.1	0.315/0.977	NA
	8-2	-6.8	0.064/0.119	Gly148
9	9-1	-7.5	0.739/0.979	Glu132
	9-2	-6.1	0.444/1.262	NA
10	10-1	-7.1	0.933/1.578	His312
	10-2	-7.0	1.240/0.298	His312
	10-3	-6.8	1.240/0.298	His312
11	11-1	-6.5	0.132/0.837	Glu132
	11-2	-6.3	0.431/0.512	Glu132/ His312

First, the control experiment proved that compound0 cannot be bound within the target binding pocket which suggests the reliability of the docking procedure and experimental data.

The results of molecular docking showed that the compounds1-11 and MurD target protein had a good binding effect and high matching degree with a binding energy between -6.1 KJ/mol and -7.5 KJ/mol. From the point of view of the overlapping similarity with the original fragment, all the poses have an average RMSD value of 0.746. This indicates a high level of alignment with the original fragment. This result is confirmed by the ligand-3LK7 interaction analysis. Most of the compounds managed to maintain the crucial interaction with Glu132, except for compounds 8 and 10. Furthermore, compounds 1,2,3,4,5,10 and 11 display several additional interactions within the binding site.

Several moieties form hydrogen bonds with the surrounding residues. To increase the binding affinity for the sequential compounds, those functional groups are selected and analyzed individually. The amine group attached to the phenyl ring is for hydrogen bond with the Thr128 and Lys311. The primary alcohol attached at the same position also interacts with Glu435 and Gly148. While the ester group firmly form a hydrogen bond with His312.

Based on the results of the above analysis and observation of the molecule position in the binding pocket, the functional groups were recombined for the second round of experiments.

Experiment Part2-

The second part of the experiment focuses on docking of new compound12-22 and observing the binding poses and the ligand-protein interaction. The best docking results obtained by Autodock vina [40,41] are shown in Table 2 and the 2D structures for the compounds are shown in the diagram. (refer to Figure14). Then the complexes of proteins and compounds were visually analyzed by Pymol2.1 and Liglplot Plus.

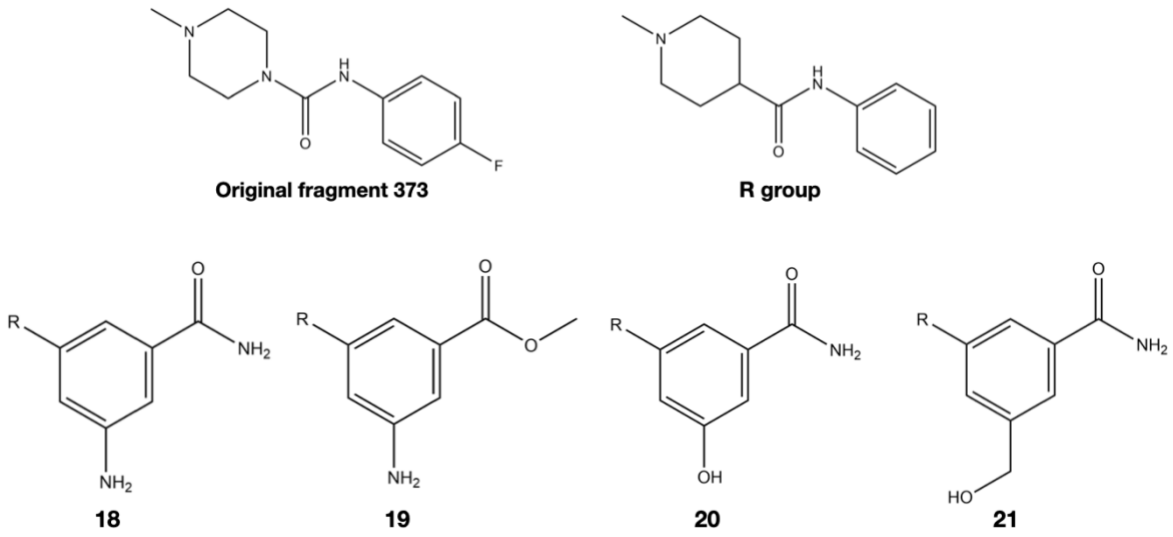

Figure14: The 2D structures for coumpounds18-21

Table2. Round2 targets protein docking results for compounds

Compound No.	Configuration Number	Binding energy	Interacted Residues
18	18-1	-7.3	Glu132(A) / Thr128(A) / Lys311(A) / His312(A)
	18-2	-7.1	Glu132(A) / Thr128(A) / Lys311(A)
	18-3	-7.1	Glu132(A) / Gly148(A) / Lys311(A) / His312(A)
19	19-1	-7.0	Glu132(A)/ Thr128(A) / His312(A) / Lys311(A)
	19-2	-6.7	Glu132(A) / Gly148(A) / His312(A) / Lys311(A)

20	20-1	-7.4	Glu132(A) / Thr128(A) / His312(A) / Lys311(A)
	20-2	-7.2	Glu132(A) / Gly148(A) / His312(A) / Lys311(A)
21	21-1	-7.3	Glu132(A) / Thr128(A) / His312(A) / Lys311(A)
	21-2	-6.9	Glu132(A) / Gly148(A) / Lys311(A)

Analysis of interaction between compound and protein

According to the docking result, compounds 18-21 have the best performance. First, they are all able to maintain the crucial hydrogen bond with Glu132 at distance between 2.80 Å and 3.06 Å. (refer to Figure15)

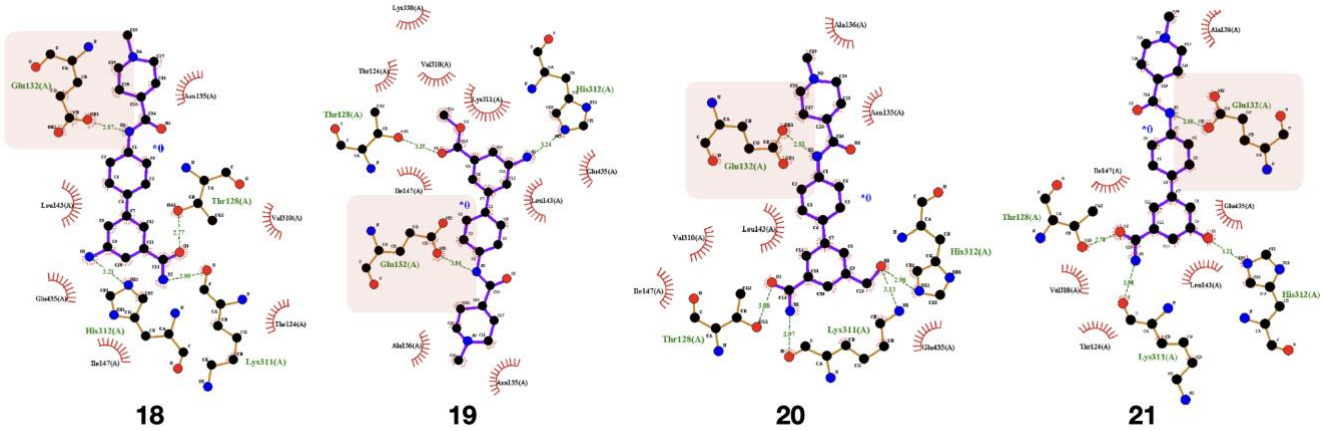

Figure15: The 2D diagram of the interactions between ligands and surrounding residues are plotted by the Ligplot+. [42,43] Dashed green lines suggest hydrogen bonds, the half-moon indicates van der Waals interactions. The pink highlighted boxes indicate the crucial hydrogen bond formed between the nitrogen atom from the central amide group and surrounding residue Glu132. Glu132(A) / Thr128(A) / Lys311(A) / His312(A)

In addition, these compounds managed to hydrogen-bonded with at least three surrounding residues within the binding site. The poses with more interactions were selected for further analysis. (refer to Figure14) For the compounds 18, within the binding site, the amine group attached to the C9 of the aromatic ring at the end is hydrogen-bonded with the imidazole from His312 with 3.21 Å. On the other side, the amine part from the amide which is attached to the C11 is hydrogen-bonded with the carboxylic acid group from Lys311 with 2.99 Å. While the oxygen atom from the same amide also interacts with the tertiary alcohol on Thr128 with 2.77 Å. In addition, the nitrogen atom from another pose generated by compound 18 interacts with the Gly148. As for compound 19, the ester group is held in the binding pocket by the hydrogen bond formed between the oxygen atom attached to the C13 and the tertiary alcohol on Thr128. The amine on the other side of the aromatic ring is also hydrogen-bonded with the imidazole from His312 with 3.24 Å. Then compound 20, which is considered the best-performed ligand, generates 5 hydrogen bonds. The primary alcohol attached to the C13 forms interactions with the imidazole from His312 and primary amine at the end of Lys311 with 2.96 Å and 3.13 Å respectively. The other end of Lys311 is the carboxylic acid which is hydrogen-bonded with the amine part of the amide group, attached to the C11. The oxygen atom from the same amide also forms a hydrogen bond with the tertiary alcohol on Thr128 with 3.08 Å. Furthermore, the amide nitrogen from another pose interacts with the Gly148. Compound 21 have a similar interaction model with compound 20. Expect a loss of a hydrogen bond between the alcohol and the Lys311. This might be due to the

shortening of the distance between the primary alcohol and aromatic ring, leading to the alteration of the binding poses.

According to the discussion, there is a huge improvement in terms of the interactions formed between the ligand and the surrounding residues, compared with the first round of experiments. These compounds managed to retain several hydrogen bonds with a fixed number of residues including Glu132(A) / Thr128(A) / Lys311(A) / His312(A) and Gly148. These hydrogen bonds play an important role in stabilizing small-molecule ligands in the cavity of anchoring proteins. Furthermore, compared with the ligands in the first round of experiments, compounds 18-21 have more consistent docking results. According to visual observation, different poses generated by the same compounds share a high level of similarity. While from the ligan-protein interaction perspective, the surrounding residues which are hydrogen-bonded with the ligands also have less difference.

The reason for these results may be that we have added functional groups that can form hydrogen bonds with surrounding residues at the positions of C11 and C9. Therefore, when docking, one of the moieties is likely to be inserted into the binding pocket. This causes a part of the other functional group to be exposed to the solution, and the other part to interact with the edge of the docking site. This structure allows ligands to form strong hydrogen bond interactions with surrounding residues in multiple directions, including the inside and the edge of the binding pocket. Which has an important contribution to the stability of small-molecule ligands in the binding pocket. (Detailed analysis is shown in Appendix 1)

The synthetic process:

When designing the compounds, whether the structure can be inserted into the binding site is our priority indeed. Meanwhile, it is also important to consider whether the reverse synthesis route of the compound is reasonable. (refer to Figure16) First, it is necessary to ensure that the reactants in the synthesis process can be found and can be purchased commercially. Secondly, if the synthesis steps can be controlled within three steps, it will be of great advantage to control the cost of subsequent experiments and ensure the purity of the final compound. In this case, the synthetic processes are shown in Figures 20-23.

The first synthesis step for compounds18-21 is the same, involving a dehydration reaction between the reactants 1-Methylpiperidine-4-carboxylic acid and 4-Bromoaniline. This reaction can be catalyzed by triethylamine and EEDQ which enables the coupling of carboxylic acids with the amine group in high yield and without racemization. While dichloromethane act as the organic solvent and the reactions are conducted at room temperature.

The next step involves the palladium-catalyzed cross-coupling reaction of Bis(pinacolato)diboron with four different reactants: [46] methyl 3-amino 5- bromobenzoate for compound18, 3-amino-5-bromobenzoate for compound 19,

methyl 3-bromo-5-(hydroxymethyl) benzoate for compound 20, 3-bromo-5-hydroxybenzoic acid for compound 21. The final products from these reactions and N-(4-Bromophenyl)-1-methyl-4-piperidinecarboxamide from the first step can be used as the reactants for the sequential Suzuki Miyaura cross-coupling reactions to give the compounds 18-21.

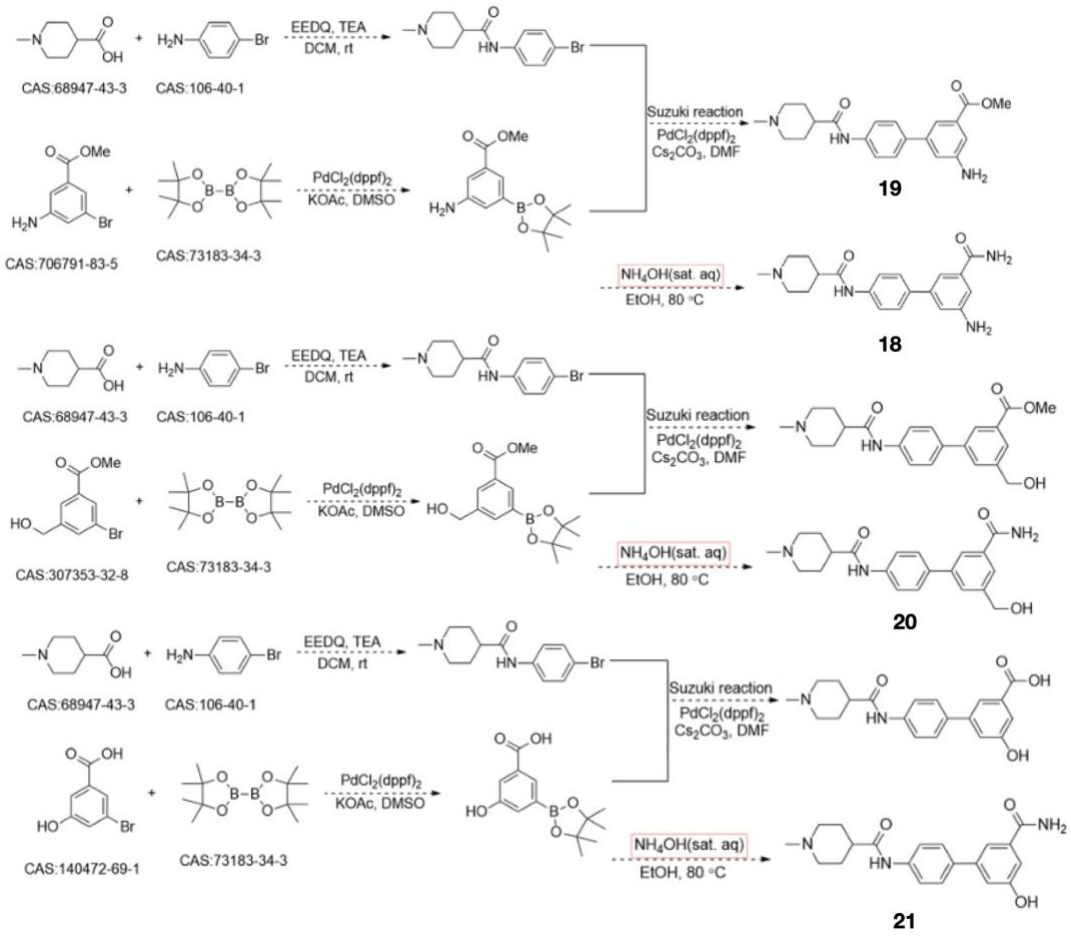

Figure:16 Chemical synthesis processes for compound 18-21

Conclusion

In this study, we briefly analyzed the main binding sites, including the ATP and substrate binding site at Mur ligase. These targets are promising due to the presence of the existing crystal structures with the substrate or ATP binding and the potential of the multiply inhibition effect. However, despite the extensive research in this field, we discovered that there are no known inhibitors that have the concentration within the therapeutic range. Therefore, we exploited an existing data set that had arisen from a fragment-based drug discovery screen. By applying X-ray crystallography, the contributors from the project managed to identify four original small-molecule fragments.

Then two rounds of silico virtual screening experiments, based on the original fragment hit MurD-x373, were conducted to optimize the binding affinity and interaction within the binding pocket. The first round of experiments gave us a general perspective on the binding mode, and a series of moieties that have the highest potential of forming interaction with the residues within the binding pocket were selected for further compound modulation. Finally, the second series of modulated compounds, consisting of the functional groups selected from the first round, were tested against MurD ligases 3LK7. The results reveal that Compounds 18-21 gave the best performance, and the chemical synthesis procedures were suggested. These compounds can be synthesized in the laboratory and the antibacterial activity can be tested in the same way as the first round of original fragments. Hopefully, provide new significant clues for the research community interested in antimicrobial drug design and pave the way for promising novel antimicrobial agents through further optimization.

Reference list

1. Tenover, F. C. Mechanisms of antimicrobial resistance in bacteria. *Am. J. Med.* **2006**, *119* (6), S3-S10. DOI: https://doi.org/10.1016/j.amjmed.2006.03.011

2. Jasovský, D.; Littmann, J.; Zorzet, A.; *et al.* Antimicrobial resistance—a threat to the world's sustainable development. *Ups. J. Med. Sci.* **2016**, *121* (3), 159-164. DOI: https://doi.org/10.1080/03009734.2016.1195900

3. Aslam, B.; Wang.; Arshad, M. I.; *et al.* Antibiotic resistance: a rundown of a global crisis. *Infect. Drug Resist.* **2018**, *11*, 1645. DOI: https://doi.org/10.2147/IDR.S173867

4. Vollmer, W.; Blanot, D.; De Pedro, M. A. Peptidoglycan structure and architecture. *FEMS Microbiol. Rev.* **2008**, *32* (2), 149-167. DOI: https://doi.org/10.1111/j.1574-6976.2007.00094.x

5. Jampilek, J. Design and discovery of new antibacterial agents: Advances, perspectives, challenges. *Curr. Med. Chem*. **2018**, *25*(38), 4972-5006. DOI: https://doi.org/10.2174/0929867324666170918122633

6. Radkov, A. D.; Hsu, Y. P.; Booher, G.; *et al*. Imaging bacterial cell wall biosynthesis. *Annu. Rev. Biochem*. **2018**, *87*, 991-1014. DOI: https://doi.org/10.1146/annurev-biochem-062917-012921

7. Matteï, P. J.; Neves, D.; Dessen, A. Bridging cell wall biosynthesis and bacterial morphogenesis. *Curr. Opin. Struct. Biol.* **2010**, *20* (6), 749-755. DOI: https://doi.org/10.1016/j.sbi.2010.09.014

8. N Sangshetti, J.; S Joshi, S.; H Patil, R.; *et al.* Mur ligase inhibitors as anti-bacterials: a comprehensive review *Curr. Pharm. Des.* **2017**, *23* (21), 3164-3196. DOI: https://doi.org/10.2174/1381612823666170214115048

9. Kouidmi, I.; Levesque, R. C.; ParadisBleau, C. The biology of Mur ligases as an antibacterial target. *Mol. Microbiol.* **2014**, *94* (2), 242-253. DOI: https://doi.org/10.1111/mmi.12758

10. Benson, T. E.; Marquardt, J. L.; Marquardt, A. C.; *et al.* Overexpression, purification, and mechanistic study of UDP-N-acetylenolpyruvylglucosamine reductase. *Biochemistry.* **1993**, *32* (8), 2024-2030. DOI: https://doi.org/10.1021/bi00059a019

11. Miller, D. J.; Hammond, S. M.; Bugg, T. D. H. Aminoalkylphosphinate inhibitors of D-Ala-D-Ala adding enzyme. *J. Chem. Soc. Perkin Trans. I*. **1998**, (1), 131-142. DOI: 10.1039/A704097K

12. Hrast, M.; Rožman, K.; Ogris, I.; *et al.* Evaluation of the published kinase inhibitor set to identify multiple inhibitors of bacterial ATP-dependent mur ligases. *J. Enzyme Inhib. Med. Chem.* **2019**, *34* (1), 1010-1017. DOI: https://doi.org/10.1080/14756366.2019.1608981

13. Smith, C. A. Structure, function and dynamics in the mur family of bacterial cell wall ligases. *J. Mol. Biol.* **2006**, *362* (4), 640-655. DOI: https://doi.org/10.1016/j.jmb.2006.07.066

14. Šink, R.; Barreteau, H.; Patin, D.; *et al.* MurD enzymes: some recent developments. *Biomol. Concepts.* **2013**, *4* (6), 539-556. DOI: https://doi.org/10.1515/bmc-2013-0024

15. Perdih, A.; Hrast, M.; Pureber, K.; *et al.* Furan-based benzene mono-and dicarboxylic acid derivatives as multiple inhibitors of the bacterial Mur ligases (MurC–MurF): experimental and computational characterization. *J. Comput. Aided Mol. Des.* **2015**, *29* (6), 541-560. DOI: https://doi.org/10.1007/s10822-015-9843-6

16. Perdih, A.; Hodoscek, M.; Solmajer, T. MurD ligase from E. coli: Tetrahedral intermediate formation study by hybrid quantum mechanical/molecular mechanical replica path method. *Proteins.* **2009**, *74* (3), 744-759. DOI: https://doi.org/10.1002/prot.22188

17. Bouhss, A.; Dementin, S.; van Heijenoort, J.; Parquet, C.; Blanot, D. MurC and MurD synthetases of peptidoglycan biosynthesis: borohydride trapping of acyl-phosphate intermediates. *Methods Enzymol.* **2002**, *354*, 189-196. DOI: https://doi.org/10.1515/bmc-2013-0024

18. Falk, P. J.; Ervin, K. M.; Volk, K. S.; *et al*. Biochemical evidence for the formation of a covalent acyl-phosphate linkage between UDP-N-acetylmuramate and ATP in the Escherichia coli UDP-N-acetylmuramate: L-alanine ligase-catalyzed reaction. *Biochemistry*. **1996**, *35* (5), 1417-1422. DOI: https://doi.org/10.1021/bi952078b

19. The PyMOL Molecular Graphics System, Version 1.2r3pre, Schrödinger, LLC.

20. Zidar, N.; Tomašić, T.; Šink, R.; *et al.* New 5-benzylidenethiazolidin-4-one inhibitors of bacterial MurD ligase: design, synthesis, crystal structures, and biological evaluation. *Eur. J. Med. Chem.* **2011**, *46* (11), 5512-5523. DOI: https://doi.org/10.1016/j.ejmech.2011.09.017

21. Kotnik, M.; Humljan, J.; Contreras-Martel, C.; *et al.* Structural and functional characterization of enantiomeric glutamic acid derivatives as potential transition state analogue inhibitors of MurD ligase. *J. Mol. Biol.* **2007**, *370* (1), 107-115. DOI: https://doi.org/10.1016/j.jmb.2007.04.048

22. Tomašić, T.; Kovač, A.; Simčič, M.; *et al.* Novel 2-thioxothiazolidin-4-one inhibitors of bacterial MurD ligase targeting D-Glu-and diphosphate-binding sites. *Eur. J. Med. Chem.* **2011**, *46* (9), 3964-3975. DOI: https://doi.org/10.1016/j.ejmech.2011.05.070

23. Tomašić, T.; Šink, R.; Zidar, N.; *et al.* Dual inhibitor of MurD and MurE ligases from Escherichia coli and Staphylococcus aureus. *ACS Med. Chem. Lett.* **2012**, *3* (8), 626-630. DOI: https://doi.org/10.1021/ml300047h

24. Zidar, N.; Tomašić, T.; Sink, R.; *et al.* Discovery of novel 5-benzylidenerhodanine and 5-benzylidenethiazolidine-2, 4-dione inhibitors of MurD ligase. *J. Med. Chem*. **2010**, *53* (18), 6584-6594. DOI: https://doi.org/10.1021/jm100285g

25. Šink, R.; Kotnik, M.; Zega, A.; *et al.* Crystallographic study of peptidoglycan biosynthesis enzyme MurD: domain movement revisited. *PLoS One.* **2016**, *11* (3), e0152075. DOI: https://doi.org/10.1371/journal.pone.0152075

26. Kumar, A.; Voet, A.; Zhang, K. Y. J. Fragment based drug design: from experimental to computational approaches. *Curr. Med. Chem.* **2012,** *19* (30), 5128-5147. DOI: https://doi.org/10.2174/092986712803530467

27. Erlanson, D. A.; McDowell, R. S.; O'Brien, T. Fragment-based drug discovery. *J. Med. Chem.* **2004,** *47* (17), 3463-3482. DOI: https://doi.org/10.1021/jm040031v

28. Congreve, M.; Chessari, G.; Tisi, D.; *et al.* Recent developments in fragment-based drug discovery. *J. Med. Chem.* **2008**, *51* (13), 3661-3680. DOI: https://doi.org/10.1021/jm8000373

29. Zoete, V.; Grosdidier, A.; Michielin, O. Docking, virtual high throughput screening and in silico fragment‐based drug design. *J. Cell. Mol. Med.* **2009**, *13* (2), 238-248. DOI: https://doi.org/10.1111/j.1582-4934.2008.00665.x

30. Davies, T. G.; Tickle, I. J. Fragment screening using X-ray crystallography. *Top. Curr. Chem.* **2011,** 33-59. DOI: https://doi.org/10.1007/128_2011_1

31. Collins, P. M.; Douangamath, A.; Talon, R.; *et al.* Achieving a good crystal system for crystallographic X-ray fragment screening. *Methods Enzymol.* **2018**, *610*, 251-264. DOI: https://doi.org/10.1016/bs.mie.2018.09.027

32. Hartshorn, M. J.; Murray, C. W.; Cleasby, A.; *et al.* Fragment-based lead discovery using X-ray crystallography. *J. Med. Chem.* **2005,** *48* (2), 403-413. DOI: https://doi.org/10.1016/bs.mie.2018.09.027

33. Schöning-Stierand, K.; Diedrich, K.; Fährrolfes, R.; *et al.* Proteins Plus: interactive analysis of protein–ligand binding interfaces. *Nucleic Acids Res.* **2020**, *48* (W1), W48-W53. DOI: https://doi.org/10.1093/nar/gkaa235

34. Fährrolfes, R.; Bietz, S.; Flachsenberg, F.; *et al.* Proteins Plus: a web portal for structure analysis of macromolecules. *Nucleic Acids Res.* **2017**, *45* (W1), W337-W343. DOI: https://doi.org/10.1093/nar/gkx333

35. Molecular Operating Environment (MOE), 2019.01; Chemical Computing Group ULC, 1010 Sherbooke St. West, Suite #910, Montreal, QC, Canada, H3A 2R7, 2021.

36. Initial MurD Hits · opensourceantibiotics/murligase Wiki. [EB/OL]. GitHub. 2021. https://github.com/opensourceantibiotics/murligase/wiki/Initial-MurD-Hits

37. MurD Round 1 · opensourceantibiotics/murligase Wiki. [EB/OL]. GitHub. 2022. https://github.com/opensourceantibiotics/murligase/wiki/MurD-Round-1.

38. New MurD synthetic targets · Issue #58 · opensourceantibiotics/murligase. GitHub. 2021. [EB/OL]. https://github.com/opensourceantibiotics/murligase/issues/58

39. O'Boyle, N. M.; Banck, M.; James, C. A.; *et al.* Open Babel: An open chemical toolbox. *J. Cheminform.* **2011** *3* (1), 1-14. DOI: https://doi.org/10.1186/1758-2946-3-33

40. Eberhardt, J.; Santos-Martins, D.; Tillack, A.; *et al.* AutoDock Vina 1.2. 0: new docking methods, expanded force field, and Python bindings. **2021**. DOI: 10.26434/chemrxiv.14774223.v1

41. Trott, O.; Olson, A. J.; AutoDock Vina: improving the speed and accuracy of docking with a new scoring function, efficient optimization, and multithreading. *J. Comput. Chem.* **2010**, *31* (2), 455-461. DOI: https://doi.org/10.1002/jcc.21334

42. Laskowski, R. A.; Swindells, M. B. LigPlot+: multiple ligand–protein interaction diagrams for drug discovery. 2011, 2778-2786. DOI: https://doi.org/10.1021/ci200227u

43. Wallace, A. C.; Laskowski, R. A.; Thornton, J. M. LIGPLOT: a program to generate schematic diagrams of protein-ligand interactions. *Protein Eng. Des. Sel*. **1995**, *8* (2), 127-134. DOI: https://doi.org/10.1093/protein/8.2.127

44. Friesner, R. A.; Banks, J. L.; Murphy, R. B.; *et al.* Glide: a new approach for rapid, accurate docking and scoring. 1. Method and assessment of docking accuracy. *J. Med. Chem.* **2004**, *47* (7), 1739-1749. DOI: https://doi.org/10.1021/jm0306430

45. Mazumder, R; Vasudevan, S; Structure-guided comparative analysis of proteins: principles, tools, and applications for predicting function. *PLoS Comput. Biol.* **2008**, *4* (9), e1000151. DOI: https://doi.org/10.1371/journal.pcbi.1000151

46. Takagi, J.; Takahashi, K.; Ishiyama, T.; *et al.* Palladium-catalyzed cross-coupling reaction of bis (pinacolato) diboron with 1-alkenyl halides or triflates: convenient synthesis of unsymmetrical 1, 3-dienes via the borylation-coupling sequence. *J. Am. Chem. Soc*. **2002**, *124* (27), 8001-8006. DOI: https://doi.org/10.1371/journal.pcbi.1000151

Appendix:

Detailed analysis for the interactions between surrounding residues of MurD ligase binding pocket and the compounds 18/19/20/21

Compound 18/configuration 1 (with binding energy=-7.3 KJ/mol)

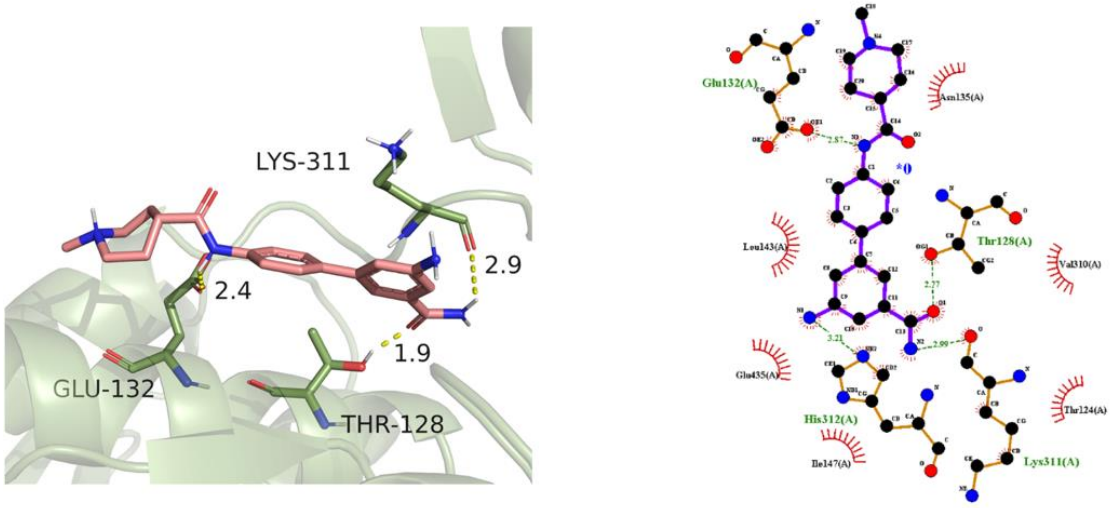

Figure:1 Left side: 2D ligand-protein interactions, dashed green lines suggest hydrogen bonds, the half-moon indicates van der Waals interactions. [44] Right side: 3D ligand-protein interactions

Within the binding site, the amine group attached to the C9 of the aromatic ring at the end is hydrogen-bonded with the imidazole from His312 with 3.21 Å. The amine part from the amide which is attached to the C11 of the aromatic ring at the end is hydrogen-bonded with the carboxylic acid group from Lys311 with 2.99 Å. While the oxygen atom from the same amide also interacts with the tertiary alcohol on Thr128 with 2.77 Å.

Compound 18 configuration 2 (with binding energy=-7.1 KJ/mol)

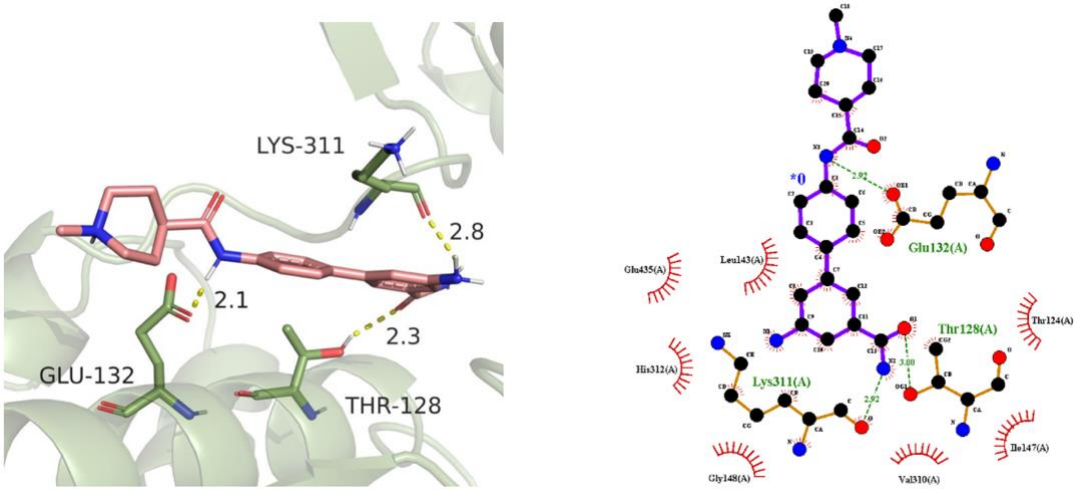

Figure:2 Left side: 2D ligand-protein interactions, Right side: 3D ligand-protein interactions

The amine part from the amide which is attached to the C11 of the aromatic ring at the end is hydrogen-bonded with the carboxylic acid group from Lys311 with 2.92 Å. While the oxygen atom from the same amide also interacts with the tertiary alcohol on Thr128 with 3.00 Å.

Compound 18 configuration 3 (with binding energy=-7.1 KJ/mol)

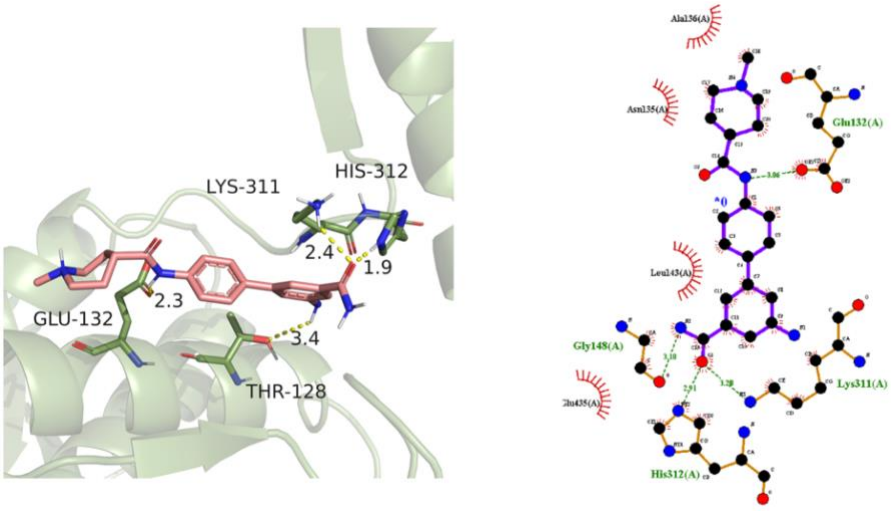

Figure:3 Left side: 2D ligand-protein interactions, Right side: 3D ligand-protein interactions

Compare with the second configuration, this pose presents an opposite direction. Where the amine is bound deep into the binding pocket and part of the amide group is exposed to the solvent. The nitrogen atom interacts with the Gly148 while the oxygen atom is hydrogen-bonded with His312 and Lys311 at 2.91 Å and 3.28 Å respectively.

Compound 19 configuration 1 (with binding energy=-7.0 KJ/mol)

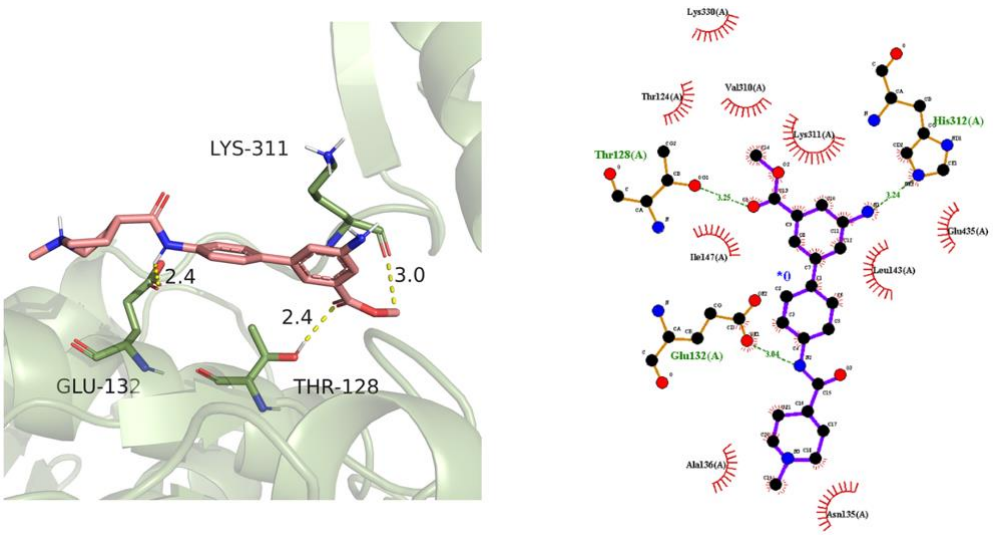

Figure:4 Left side: 2D ligand-protein interactions, Right side: 3D ligand-protein interactions

Within the binding site, the ester group is held in the binding pocket by the hydrogen bond formed between the oxygen atom attached to the C13 and the tertiary alcohol on Thr128. The amine on the other side of the aromatic ring also hydrogen-bonded with the imidazole from His312 with 3.24 Å.

Compound 19 configuration 2 (with binding energy=-6.7 KJ/mol)

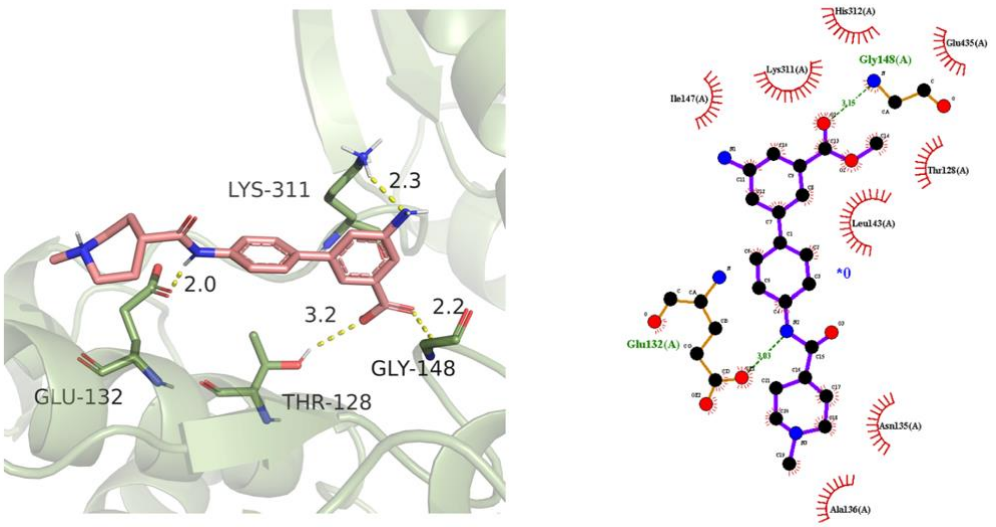

Figure:5 Left side: 2D ligand-protein interactions, Right side: 3D ligand-protein interactions

Within the binding site, the ester group is held in the binding pocket by the hydrogen bond formed between the oxygen atom attached to the C13 and the tertiary alcohol on Thr128. The amine on the other side of the aromatic ring also hydrogen-bonded with the imidazole from His312 with 3.24 Å.

Compound 20 configuration 1 (with binding energy=-7.4 KJ/mol)

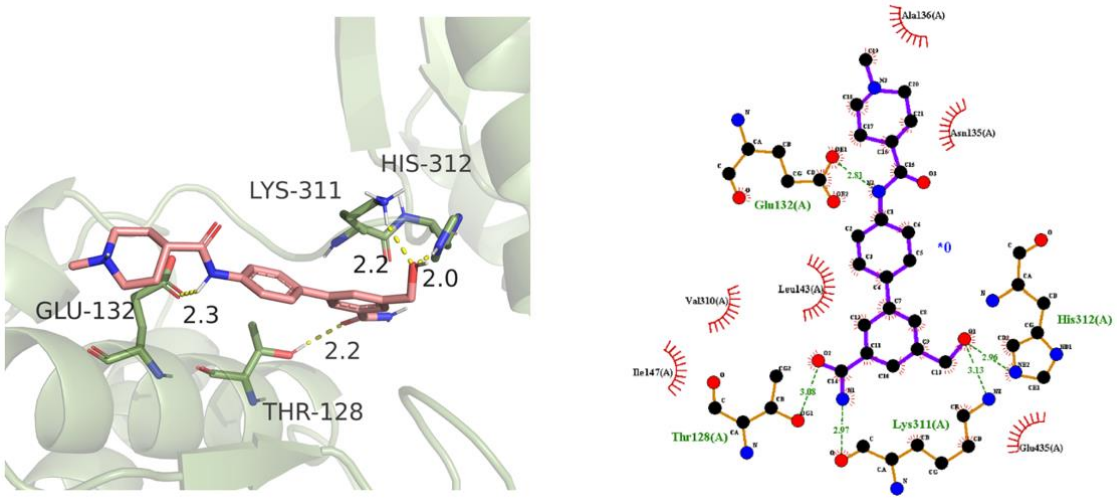

Figure:6 Left side: 2D ligand-protein interactions, Right side: 3D ligand-protein interactions

The primary alcohol attached to the C13 forms interactions with the imidazole from His312 and primary amine at the end of Lys311 with 2.96 Å and 3.13 Å respectively. The other end of Lys311 is the carboxylic acid which is hydrogen-bonded with the amine part of the amide group, attached to the C11. The oxygen atom from the same amide also forms a hydrogen bond with the tertiary alcohol on Thr128 with 3.08 Å.

Compound 20 configuration 2 (with binding energy=-7.2 KJ/mol)

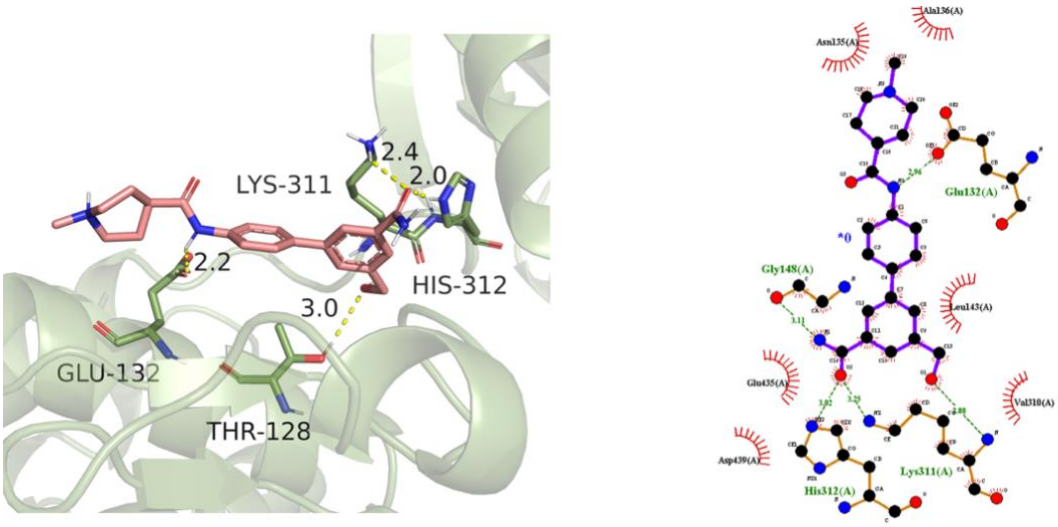

Figure:7 Left side: 2D ligand-protein interactions, Right side: 3D ligand-protein interactions

Within the binding site, the amine part from the amide group which is attached to the C14 is hydrogen-bonded with the carboxylic acid group from Gly148 with 3.11 Å. While the oxygen atom from the same amide interacts with the imidazole from His312 with 3.02 Å, meanwhile this moiety also interacts with the carboxylic acid group from Lys311 with 3.25 Å. The other side of the aromatic ring is also connected with Lys311 by the interaction between tertiary amine and primary alcohol attached to the C13 with 2.88 Å.

Compound 21 configuration 1 (with binding energy=-7.3 KJ/mol)

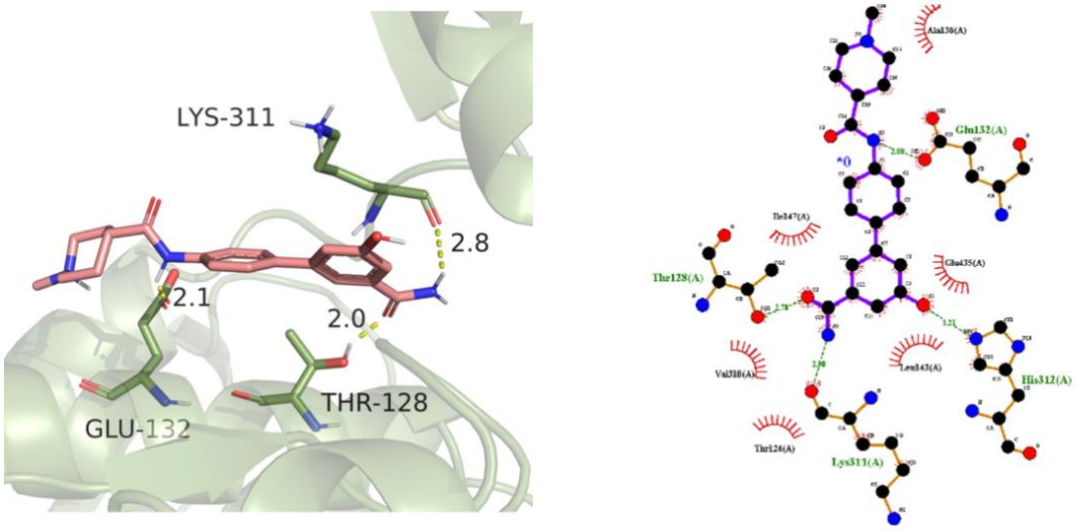

Figure:8 Left side: 2D ligand-protein interactions, Right side: 3D ligand-protein interactions

Within the binding site, the secondary alcohol attached to the C9 forms a hydrogen bond with the imidazole from His312 at 3.21 Å. The amine part from the amide which is attached to the C11 is hydrogen-bonded with the carboxylic acid group from Lys311 with 2.98 Å. While the oxygen atom from the same amide also interacts with the tertiary alcohol on Thr128 with 2.78 Å.

Compound 21 configuration 2 (with binding energy=-7.3 KJ/mol)

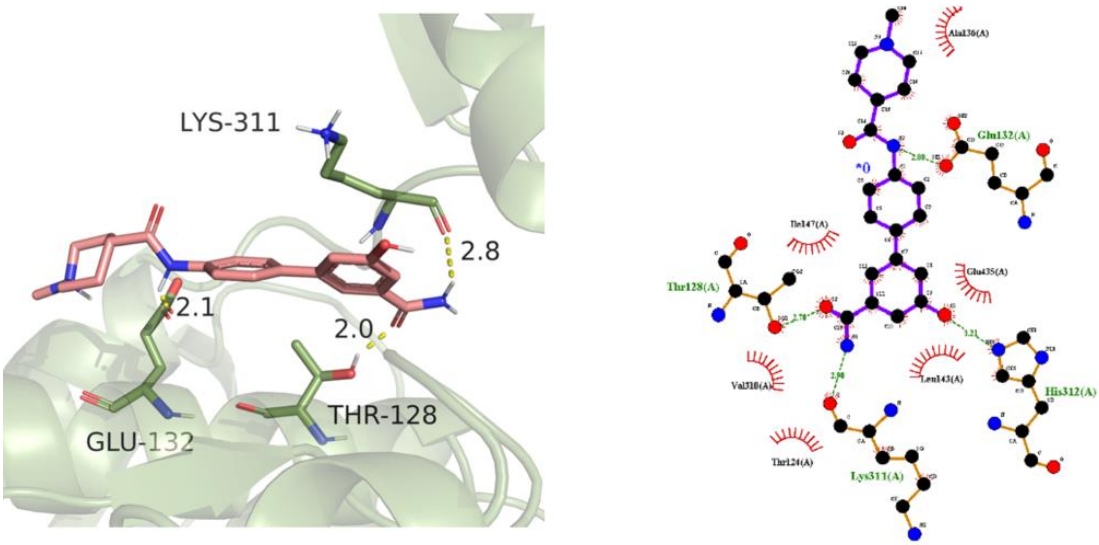

Figure:9 Left side: 2D ligand-protein interactions, Right side: 3D ligand-protein interactions

Within the binding site, the amine part from the amide which is attached to the C11 is hydrogen-bonded with the carboxylic acid group from Lys311 with 2.98 Å. While the oxygen atom from the same amide also interacts with the tertiary alcohol on Thr128 with 2.78 Å. For the part where is exposed to the solvent, the amide moiety located in-between piperidine and the middle aromatic ring is held in place by the hydrogen bond with the carboxylic acid of Glu132 with 3.04 Å. This carboxylic acid is also hydrogen-bonded with the nitrogen at the piperidine ring with 3.10 Å.